Solid State Ionics 181 (2010) 53–58

Contents lists available at ScienceDirect

Solid State Ionics

journal homepage: www.elsevier.com/locate/ssi

The oxygen permeation characteristics of $Bi_{1-x}Sr_xFeO_3$ mixed ionic and electronic conducting ceramics

K. Brinkman [a,*], T. Iijima [b], H. Takamura [c]

[a] Materials Science and Technology Directorate, Savannah River National Laboratory (SRNL), Aiken, SC, 29808, USA
[b] Research Center for Hydrogen Industrial Use and Storage, National Institute of Advanced Industrial Science and Technology (AIST), Tsukuba Central 5, Tsukuba, Ibaraki 305-8565, Japan
[c] Department of Materials Science, Graduate School of Engineering, Tohoku University, Sendai 980-8579, Japan

ARTICLE INFO

Article history:
Received 31 July 2009
Received in revised form 1 November 2009
Accepted 29 November 2009

Keywords:
Oxygen permeation
Conductivity
Mixed conducting oxide

ABSTRACT

The perovskite oxides in the system $Bi_{1-x}Sr_xFeO_{3-\delta}$ ($x=0.05$, 0.15, 0.3, 0.6, and 0.8) were characterized in the intermediate temperature range (650 to 800 °C) by oxygen permeation and electrical conductivity measurements. The samples exhibited a single phase perovskite structure with a decreasing lattice constant with increasing Sr concentration and a structural change from rhombohedral to cubic at $x \geq 0.3$. Mixed conductivity was confirmed in all samples with maximum flux levels on the order of 0.11 μmol/cm^2 s at 800 °C for the $x=0.8$ composition. Materials studied displayed p-type conductivity over the oxygen partial pressure range present in permeation measurements (0.21 to 10^{-6} atm). A local maximum of oxygen flux and ionic conductivity was found near $x=0.3$.

1. Introduction

The development and characterization of mixed electronic and ionic conducting oxide materials are of current importance in the fields of gas sensing [1], solid oxide fuel cells [2], oxygen production [3], and hydrogen/syngas generation via the partial oxidation of methane [3,4]. Single phase materials displaying high oxygen flux are based on the ABO_3 perovskite structure with appropriate A and B site doping to enhance oxygen vacancy concentration, conductivity as well as phase stability. Teraoka initially investigated a wide range of compositions based on the parent compound $SrFeO_{3-\delta}$, including A site La doping and B site Co doping [5]. It was found that additions of La^{+3} on the Sr^{+2} site were detrimental to oxygen flux properties, emphasizing the impact of oxygen vacancy concentration controlled by acceptor doping. The highest flux values were found with high levels of Co doping on the B site (80%), with just enough Fe remaining in order to stabilize the perovskite phase. The level of oxygen flux on the order of 1 μmol/cm^2 s at 800 °C for 1 mm thick ceramics for this material system, first explored over 20 years ago, is still among the highest yet observed. However, pure $SrFeO_{3-\delta}$ (SFO) undergoes a series of well known phase transformations to a vacancy ordered brownmillerite phase at low PO_2 levels where oxygen is removed from the perovskite lattice [6,7]. In addition, high levels of Co doping led to materials with high thermal expansion coefficients due the small ionic radius of reduced Co.

The thermal expansion characteristics of mixed conductors are important for applications where the anode and electrolyte (ceria or zirconia) should have similar thermal expansion as well as for the new generation of micro solid oxide fuel cells (SOFC's) and Si integrated sensors based on Si thin film technology [8,9]. Investigations into Co free materials has resulted in the discovery of compositions such as $BaCe_xFe_{1-x}O_{3-\delta}$ (BCF) [10], $La_{1-x}Sr_xGaO_{3-\delta}$ [11,12], $CaTi_{1-x}Fe_xO_{3-\delta}$ [13,14]. The two latter compositions displayed low oxygen flux values two orders of magnitude less than SFO (less than 0.06 μmol/cm^2 s at 900 °C and 1 mm thickness). The flux of BCF was observed to be only one order of magnitude below SFO (0.15 μmol/cm^2 s at 800 °C) however, this composition was difficult to prepare as phase pure perovskite, and exists as Ce and Fe rich phases where only the Fe phase contributes to the oxygen flux.

Bismuth containing compounds have also been the subject of investigation for electrolytes [15] and mixed composites for oxygen permeation [16] due to the high ionic conductivity of bismuth oxide. Bismuth ferrites $BiFeO_3$ and $Bi_2Fe_4O_9$ have been investigated as gas sensors [17] with limited success. A recent report indicated that small levels of acceptor doping with Ca or Sr in $BiFeO_3$ results in ceramics with appreciable oxygen permeation properties while increasing the maximum operating temperature and aiding in the elimination of commonly observed secondary phases often observed in pure $BiFeO_3$ [18]. Bismuth ferrite has a distorted perovskite lattice with R3c rhombohedral parameters a 3.958 Å and α 89.3 [19] similar to the cubic perovskite structure of $SrFeO_x$ ($2.9 \leq x \leq 3$) with Pm3m symmetry and a lattice parameter a 3.8553 Å [20]. In addition to the oxygen permeation properties in [18], the role of dopants has most recently been explored as a way to control the electric modulation of conduction in multiferroic films [21], and as a method to stabilize the

* Corresponding author.
E-mail address: kyle.brinkman@srnl.doe.gov (K. Brinkman).

0167-2738/$ – see front matter © 2009 Elsevier B.V. All rights reserved.
doi:10.1016/j.ssi.2009.11.016

$BiFeO_3$ phase over $Bi_2Fe_4O_9$ like structures closely related in free energy [22].

A series of perovskite oxides $Bi_{1-x}Sr_xFeO_3$ was proposed to have high oxygen flux levels [23], however there are contradictory reports in the literature. Li examined the oxygen permeation properties from 800 °C to 1000 °C of this system with $x=0.5$, 0.7, and 0.9. It was observed that the oxygen flux performance of these compositions was similar at 800 °C, with Bi rich compositions showing higher flux at higher temperatures up to 1000 °C . In the same report, a new phase was reported $Sr_{10-n/2}Bi_nFe_{20}O_{3-\alpha}$ with $n=10$. This phase was indexed to the orthorhombic system, and displayed oxygen flux values of 0.67 μmol/cm^2 s at 850 °C, over two times higher than the standard $Bi_{1-x}Sr_xO_3$ system [24]. However, in a separate report, no such phase was reported and detailed structural studies indicated the presence of a single phase over the composition range $x=0.2$ to $x=0.67$ [25]. A further anomaly is the order of magnitude difference in the reported values of oxygen flux for the same composition given in Refs. [24] and [26].

The focus of this manuscript is on the oxygen permeation properties and conductivity of $Bi_{1-x}Sr_xFeO_3$ over a wide composition range $x=0.05$ to $x=1.00$. In the following it is shown that (i) the samples exhibited single phase perovskite over the whole composition range with the lattice constant decreasing with increasing Sr concentration, (ii) oxygen flux measurements confirming mixed conductivity in all the samples reaching a maximum of 0.11 μmol/cm^2 s at 800 °C for $x=0.8$, (iii) p-type conductivity was observed over the oxygen partial pressure range of oxygen permeation measurements (0.21 to 10^{-6}) (iv) oxygen flux versus Sr concentration displayed an intermediate maximum at $x=0.3$ thus showing two distinct regimes of oxygen flux and ionic conductivity behavior. This work examines the broad compositional range from $x=0.05$ to $x=1.00$ in the $Bi_{1-x}Sr_xFeO_3$ system, and puts the structure, electronic and ionic conductivity behavior in perspective with the select compositions previously reported.

2. Experimental

$Bi_{1-x}Sr_xFeO_3$ acceptor doped ceramics were prepared Sr at $x=0.05$ to $x=1.00$. Stoichiometric amounts of Bi_2O_3, Fe_2O_3, and SrO (High Purity Chemical Co., Japan) were weighed and ball milled in ethanol for 24 h, dried and calcined at temperatures from 750 °C to 1100 °C for 5 h in air. After a second grinding and sieving step, the ceramics were mixed with a binder and uniaxially pressed into pellets of 16 mm diameter with a force of 20 kN for several minutes. The ceramic sintering temperature varied with the dopant concentration, from 920 °C ($x=0.05$) to 1300 °C ($x=1$). All sintered samples had relative densities greater than 88%.

The crystal structure of the calcined powders and sintered ceramics were examined by X-ray diffraction on a Philips X-pert and the microstructure was determined by SEM (Jeol) after polishing followed by thermal etching. The lattice parameters of the powder patterns in the range 20 to 70° two-theta were calculated from the peak maximum using regression analysis following Cohen's method [27,28].

Oxygen flux measurements were made on polished ceramic samples of nominal thickness 1 mm with a diameter of 13 mm. Ceramic samples were placed between two quartz tubes using a glass ring (melting point 620 °C) for gas sealing, and a metal spacer with a diameter of 5 mm to control the area of gas flux. Flowing He (20 sccm) was supplied to the permeate side of the ceramic membrane while air at 1 atm was supplied to the feed side. The gas concentration of O_2 and N_2 was measured on the membrane permeate side using a gas chromatograph (GC323; GL Sciences Co., Ltd). The leakage of oxygen was calculated by measuring the volume of N_2 gas from air on the permeate side. The oxygen permeation flux was corrected using the total measured oxygen on the permeate side minus the physical leakage of oxygen. The leakage was below 3% in all samples measured in this study.

Electrical conductivity measurements were performed using a DC four probe method in the temperature range 600 to 800 °C under a P(O_2) range of 0.21 to 10^{-10} atm using CO–CO_2 gas mixtures. The sample ionic conductivity was estimated using the Wagner relation [29] assuming that in 1 mm thick membranes the bulk transport is the rate determining step(confirmed in Ref. [18] for low Sr concentrations), and electronic conductivity is greater than the ionic conductivity resulting in the relation:

$$JO_2 = \frac{RT\sigma_i}{16F^2L}\ln\frac{p_h}{p_l} \quad (1)$$

where JO_2 is the oxygen permeation flux (mol/m^2 s), R is the gas constant (8.314 J/mol K), T is the temperature (K), F is the Faraday constant (96485 C/mol), L the thickness of the membrane (m), p_h and p_l are the partial oxygen pressures on the feed and permeate sides respectively. The actual concentration of gas at the permeate side (p_l) as measured by the GC was used to estimate the oxygen partial pressure "driving force" for ionic conduction.

3. Results

3.1. Structure

Fig. 1 displays the X-ray diffraction patterns of calcined powders with varying strontium contents from $x=0.05$ to 0.8. A close up view of the region near 50° two-theta reveals the crossover from rhombohedral at Sr doping levels up to $x=0.3$ to a purely cubic structure. No secondary phases of $Bi_2Fe_4O_9$ or Bi_25FeO_{39} were observed over the entire composition range studied which is in agreement with previous work reporting enhanced $BiFeO_3$ phase stability with A site dopants Ca and Sr [18].A recent study in Sr doped BFO thin films found that Sr was indeed substituted at the A site in the perovskite structure [30]. The pseudocubic/cubic lattice parameter as a function of Sr concentration from this study that is compared with literature values from three different prior reports [20,24,25] is displayed in Fig. 2. The present work investigating the complete range of Sr doping is in close agreement with other reports on the material system and reveals a sharp drop in the lattice parameter concomitant with the rhombohedral to cubic phase transition near 30% Sr, followed by the lattice parameter decrease to the $SrFeO_3$ endmember. Previous structural studies have indicated that the lattice parameter decreased with increasing x. In addition, Mössbauer studies indicated that the iron remained in the tri-valent state even with Sr substitution up to $x=0.67$ [25]. The relevant processing conditions including calcination and sintering temperature along with X-ray diffraction determined structural parameters are summarized in Table 1. The SEM determined microstructural features of sintered ceramics with varying strontium content are shown in Fig. 3. The grain size is seen to increase with increasing strontium content, however this is due to the increase in the calcination and sintering temperatures utilized from 920 °C with $x=0.05$ to 1100 °C with $x=0.8$ resulting in a nominal grain size increase from 1 to 5 μm. The micron size grains found in all of the reported samples indicate that the oxygen transport properties reported in the subsequent section are bulk properties of the system and are not affected by space charge effects found in "nanoscale ionic" conduction [31].

3.2. Oxygen permeation properties

A representative plot of the oxygen flux as a function of measurement time and temperature is given for $BiFeO_3$ with 80% Sr in Fig. 4. The flux is seen to be stable with time over a one hour period of measurement at temperatures below 800 °C. At 800 °C, the flux initially reaches values of 0.11 (μmol/cm^2 s) and decreases to 0.083(μmol/cm^2 s) after 1 h of measurement. This composition was sintered in air at temperatures

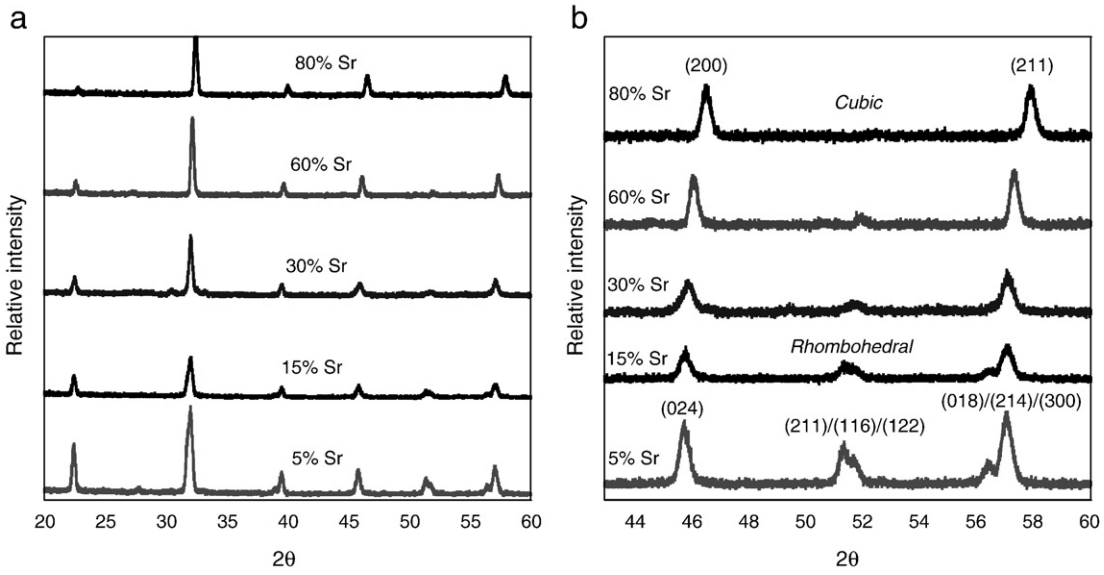

Fig. 1. (a) X-ray diffraction patterns of $Bi_{1-x}Sr_xFeO_3$ calcined powders with varying Sr contents from $x=0.05$ to $x=0.8$ (5 to 80% Sr). (b) Detail range where rhombohedral to cubic transformation is seen at dopant concentration higher than $x=0.3$.

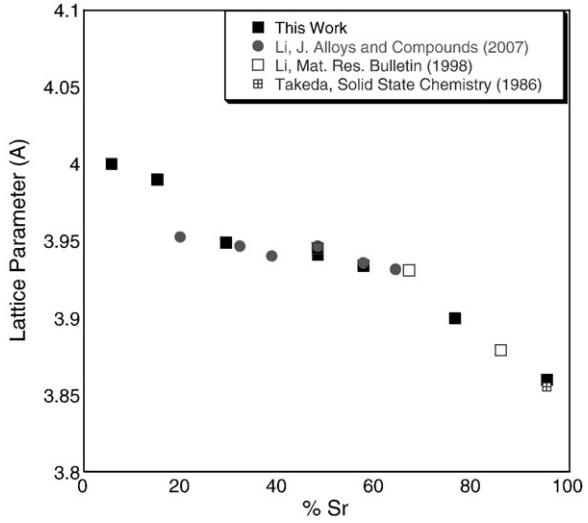

Fig. 2. X-ray determined cubic/pseudocubic lattice parameter a (Å) as a function of Sr concentration as determined in this study compared with literature values in references [20,24,25].

Table 1
Sample preparation conditions and X-ray determined structural characteristics (ambient temperature) of $Bi_{1-x}Sr_xFeO_3$.

Sample	T°C calcine (time h)	Structure	Volume	ρ_{xray}[28]	ρ_{meas} (density %)
%Sr	T°C sinter (time h)	Lattice parameter a (Å)	Å^3	(g/cm^3)	(g/cm^3)
5	750 (5)	Rhombohedral			
	920 (5)	4.0, $\alpha=89.4$ (deg)	63.98	7.96	7.81 (98)
15	750 (5)	Rhombohedral			
	950 (5)	3.99, $\alpha=89.5$ (deg)	63.51	7.71	6.99 (91)
30	800 (5)	Rhombohedral/cubic			
	1000 (5)	3.95 $\alpha\sim90$ (deg)	61.63	7.45	6.99 (94)
50	900 (5)	Cubic			
	1100 (5)	3.94	61.16	6.84	6.58 (96)
60	1000 (5)	Cubic			
	1100 (5)	3.93	60.70	6.57	5.91 (90)
80	1000 (5)	Cubic			
	1100 (5)	3.90	59.32	6.04	5.33 (88)
100	1000 (5)	Cubic			
	1300 (5)	3.86	57.51	5.53	4.65 (84)

greater than 1000 °C. Neither the temperatures reached during the permeation measurements, nor the air/He environment was expected to alter the microstructure or phase assemblage of the system. Indeed, neither microstructural changes nor secondary phase formation was observed in post experiment specimen characterization. It is hypothesized that the reduction in flux which only occurred at elevated flux levels near 0.1 (μmol/cm^2 s) was a result of the oxygen concentration on the permeate side of the membrane leading to a reduced driving force for oxygen permeation through the bulk membrane. In order to compare the flux between different compositions and temperatures, the average flux over the 1 hour measurement time was chosen to be representative for the following discussion.

It has been previously observed in the BFO system that for membrane thickness on the order of 1 mm, a decrease in the film thickness resulted in increasing oxygen flux. This observation indicates that bulk diffusion of oxygen is the dominant mechanism under these experimental conditions [18]. In order to compare the nominal flux values for different strontium dopant concentrations, the oxygen flux for all membranes in this study were normalized to 1 mm thickness. Fig. 5 displays the oxygen flux versus temperature and dopant concentration. The oxygen flux is seen to increase with increasing temperature across the range of doping. An anomaly in the oxygen flux versus strontium dopant measured at 800 °C is seen in Fig. 5 where the flux is seen to increase from low doping levels up to 30% followed by a decrease between 30 and 60% before further increase at 80 and 100% doping levels (corresponding to pure $SrFeO_3$). A summary of the oxygen flux and measurement parameters in this study as compared to previous literature is outlined in Table 2.

3.3. Conductivity

The conductivity versus temperature and oxygen partial pressure for $BiFeO_3$, 5% Sr and $SrFeO_3$ [5] is displayed in Fig. 6. The decrease in conductivity as oxygen partial pressure decreases from air (PO_2 0.2 atm) to values near PO_2 10^{-8} is indicative of p-type conductivity in the system via the defect chemistry described in Eq. (2) where an increase in oxygen partial pressure leads to an increase in holes (p-type charge carriers) and conductivity of the material.

$$1/2O_2 + Vo^{\cdot\cdot} \rightarrow Oo^{x} + 2h^{\cdot} \quad (2)$$

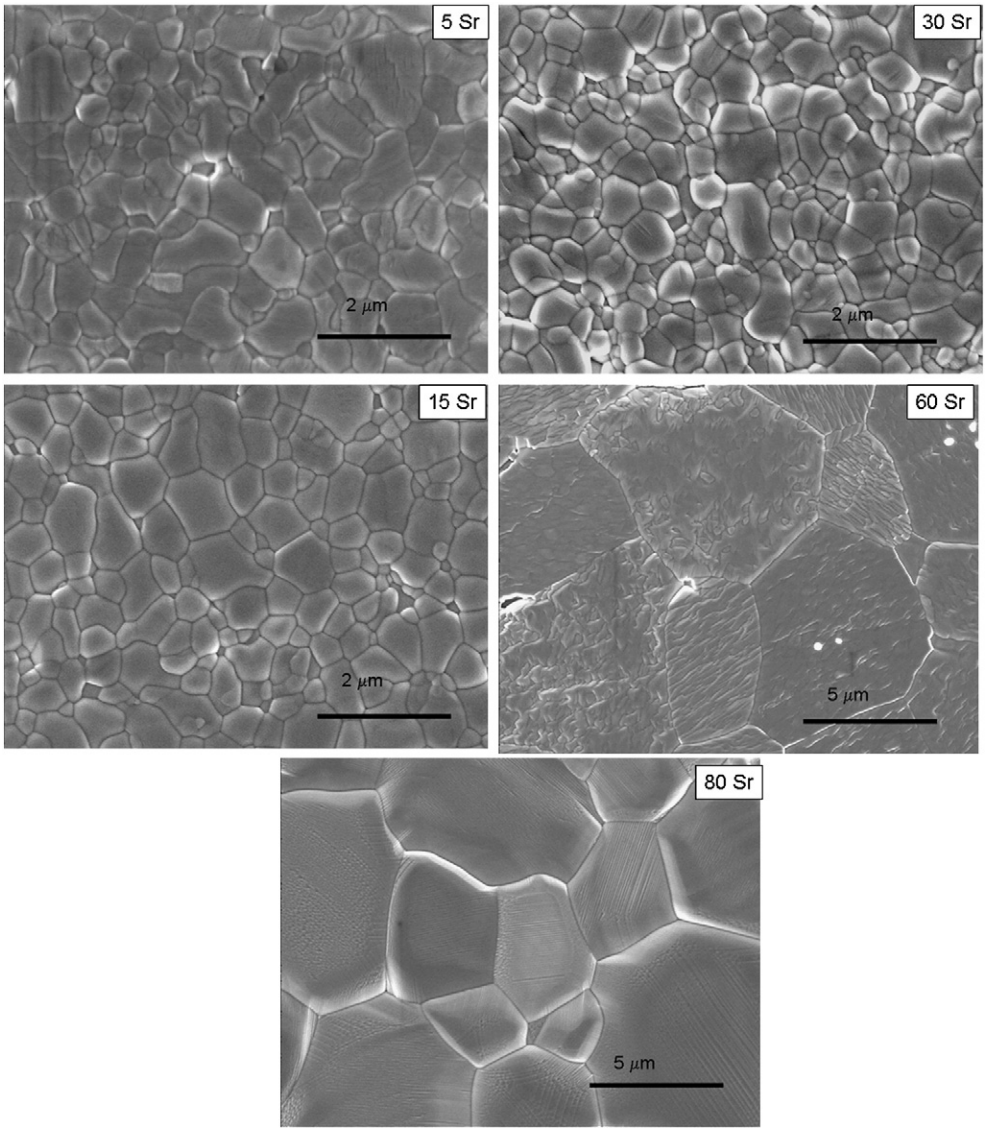

Fig. 3. SEM photos of sintered ceramics with 5, 15, 30, 60 and 80% Sr additions.

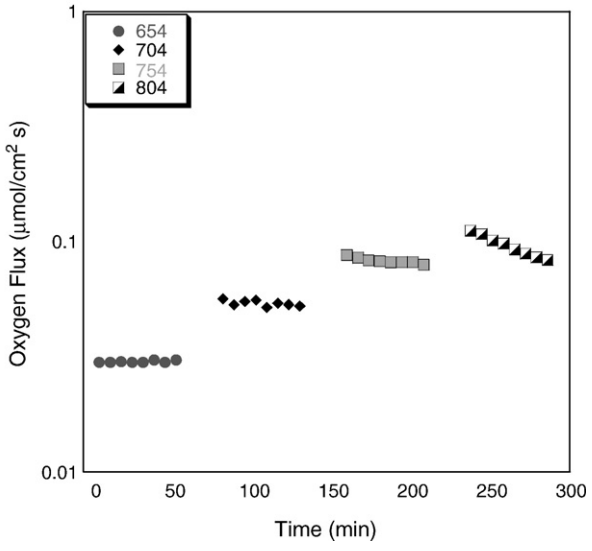

Fig. 4. Oxygen flux [μmol/cm^2] as a function of measurement time (min) at temperatures from 650 °C to 800 °C of $Bi_{0.8}Sr_{0.2}FeO_3$ or 80% Sr (1.17 mm thickness).

The effect of doping with low levels of acceptor dopant Sr^{+2} is to increase the oxygen vacancy concentration according to $2Vo^{\cdot\cdot} = [Sr + 2_{Bi+3}]'$, which leads to an overall increase in the total conductivity at high oxygen partial pressures as seen in Eq. (2). The p-type conductivity observed in $SrFeO_3$ is due to B site reduction of iron according to $2Vo^{\cdot\cdot} = [Fe + 3_{Fe+4}]'$ which results in an order of magnitude increase in the conductivity under air at temperatures in excess of 700 °C over 5% Sr doped BFO, and a nearly two order of magnitude increase over pure BFO [32]. The ionic conductivity at 800 °C for $SrFeO_3$ is known to be near 0.1 S/cm which is significantly less than the total conductivity in air environments [33]. The conditions of oxygen permeation used in this study (air and helium sweep gas) correspond to an approximate range of partial pressures from 0.21 to 10^{-6} atm PO_2. This regime seen in Fig. 6 is clearly in the p-type carrier regime where $\sigma_{electronic} \gg \sigma_{ionic}$ which permits the use of Eq. (1) to estimate the ionic conductivity across the doping range used in this study. The results of these estimates are shown in Fig. 6b showing the ionic conductivity versus Sr dopant concentration at 800 °C. Since these estimates were derived from oxygen flux measurements along with Eq. (1), the same qualitative shape is found when looking at oxygen flux and ionic conductivity as a function of doping. Even with the iron remaining in the tri-valent state with Sr substitution up to $x = 0.67$ [25], it is clear that a large

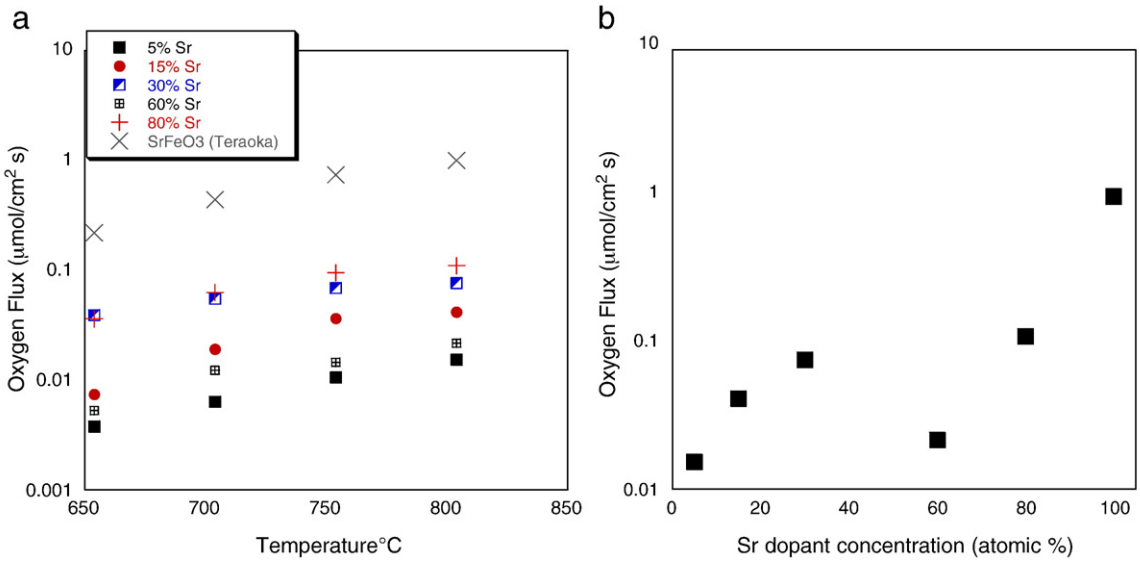

Fig. 5. (a) Oxygen flux [μmol/cm^2 s] normalized to 1 mm thickness versus temperature for $Bi_{1-x}Sr_xFeO_3$ ceramics with increasing Sr doping level. (b) Oxygen flux versus Sr dopant concentration at 800 °C. $SrFeO_3$ data from Teraoka [5].

Table 2
Summary of the oxygen flux characteristics of $Bi_{1-x}Sr_xFeO_3$ materials in this work as compared with literature values in references [24,26].

Sample	JO_2 μmol/cm^2 s	Temp°C	PO_2 difference	Reference
$Bi_{0.85}Sr_{0.15}FeO_3$	0.042	800	Air to He	This work
$Bi_{0.7}Sr_{0.3}FeO_3$	0.077	800	Air to He	This work
$Bi_{0.4}Sr_{0.6}FeO_3$	0.022	800	Air to He	This work
$Bi_{0.2}Sr_{0.8}FeO_3$	0.11	800	Air to He	This work
$Bi_{0.3}Sr_{0.7}FeO_3$	0.018	850	Air to He	[26]
$Bi_{0.3}Sr_{0.7}FeO_3$	0.16	850	Air to Ar	[24]
$Bi_{0.5}Sr_{0.5}FeO_3$	0.26	850	Air to Ar	[24]

number of oxygen vacancies are present at Sr doping levels in the 30% to 60% regime. At these levels of oxygen deficiency, superlattice ordering is favored and the well known brownmillerite structure $A_2B_2O_5$ is often observed at elevated temperature [7,34]. The ordered nature of this structure leads to lower levels of oxygen ion conductivity and oxygen permeation. At present there is no data on high temperature structural information of $Bi_{1-x}Sr_xO_3$ in gas ambient relevant to oxygen permeation measurements. Thermal analysis techniques such as thermogravimetric analysis–differential thermal analysis (TGA/DTA) in conjunction with temperature programmed desorption (TPD) as well as structural information from high temperature X-ray diffraction (XRD) are the logical next steps for the further investigation of this system. Therefore it is consistent with the broad knowledge base developed in complex oxide systems that the onset of defect interactions grows with increased defect concentrations, and that the observed decreases in oxygen flux and ionic conductivity occurring at doping levels from 30% to 60% are due to the ordering and/or concomitant defect associations. Further work is currently underway to examine these issues.

4. Conclusion

The perovskite oxides in the system $Bi_{1-x}Sr_xFeO_{3-\delta}$ ($x = 0.05$, 0.15, 0.3, 0.6, and 0.8) exhibited a single phase perovskite structure

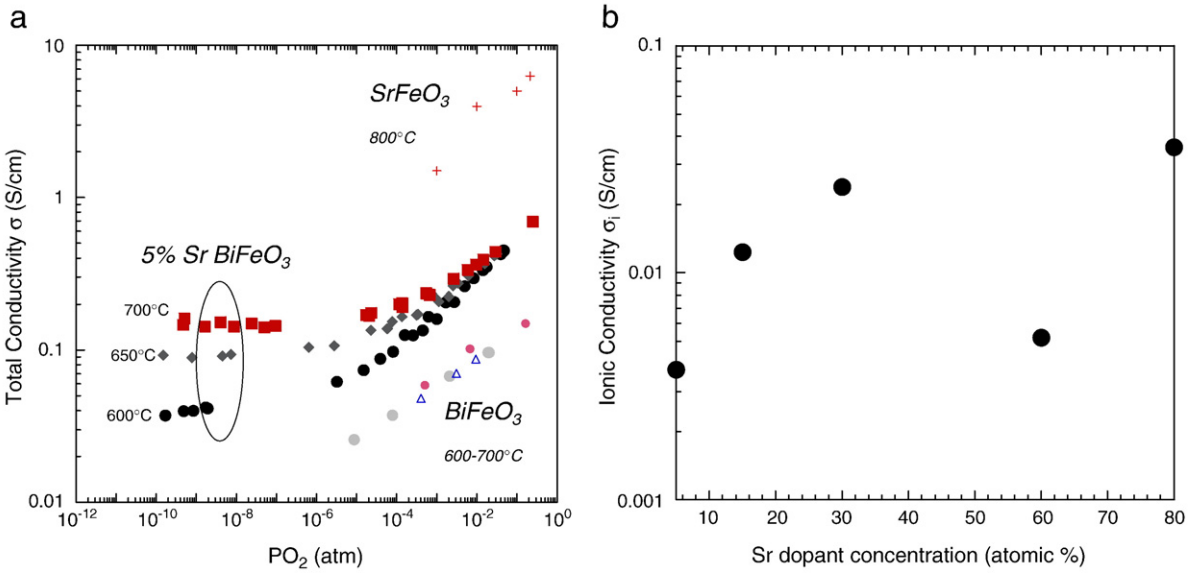

Fig. 6. (a) The total conductivity of BFO ceramics as a function of temperature and oxygen partial pressure $SrFeO_3$ data from Poulsen [32]. (b) Ionic conductivity calculated from oxygen flux data using equation (1).

with a decreasing lattice constant with increasing Sr concentration and a structural change from rhombohedral to cubic at $x \geq 0.3$. Mixed conductivity was confirmed in all samples with maximum flux levels on the order of 0.11 μmol/cm^2 s at 800 °C for the $x = 0.8$ composition. Compositions studied displayed p-type conductivity over the oxygen partial pressure range present in permeation measurements (0.21 to 10^{-6} atm). A local maximum of oxygen flux and ionic conductivity was found near $x = 0.3$ which is consistent with defect ordering and association observed in similar complex oxide systems.

Acknowledgments

The authors acknowledge JSPS for funding support, and the SRNL LDRD program for the support of electronic ceramics for energy conversion applications.

References

[1] J. Sprague, O. Porat, H. Tuller, Sensors and Actuators B 35 (1996) 348.
[2] Z. Shao, S. Haile, Nature 431 (2004) 170.
[3] P. Dyer, R. Richards, S. Russek, D. Taylor, Solid State Ionics 134 (2000) 21.
[4] H. Takamura, Y. Aizumi, A. Kamegawa, M. Okada, Journal of Fuel Cell Science and Technology 3 (2006) 175.
[5] Y. Teraoka, H. Zhang, S. Furukawa, N. Yamazoe, Chemistry Letters (1985) 1743.
[6] M. Patrakeev, I. Leonidov, V. Kozhevnikov, Solid State Sciences 6 (2004) 907.
[7] H. Bouwmeester, Catalysis Today 82 (2003) 141.
[8] A. Jankowski, J. Hayes, R. Graff, J. Morse, Materials Research Society Symposium Proceedings 730 (2002).
[9] S. Ray Mermet, P. Muralt, Materials Research Society Symposium Proceedings 972 (2007) AA07.
[10] X. Zhu, H. Wang, W. Yang, Chemical Communications 1120 (2004).
[11] M. Schwartz, J. White, A. Sammels, US Pat., 6, 214, 757 (2001).
[12] T. Ishihara, M. Honda, T. Shibayama, H. Minami, H. Nishiguchi, Y. Takita, Journal of the Electrochemical Society 145 (1998) 3177.
[13] F. Figueiredo, V. Kharton, A. Viskup, J. Frade, Journal of Membrane Science 236 (2004) 73.
[14] F. Figueiredo, J. Waerenborgh, V. Kharton, H. Nafe, J. Frade, Solid State Ionics 156 (2003) 371.
[15] N. Jiang, E. Wachsman, S. Jung, Solid State Ionics 150 (2002) 347.
[16] E. Capoen, M. Steil, G. Nowogrocki, M. Malys, C. Pirovano, A. Lofberg, E. Bordes-Richard, J. Boivin, G. Mairesse, R. Vannier, Solid State Ionics 177 (2006) 483.
[17] A. Poghossian, H. Abovian, P. Avakian, S. Mkrtchian, V. Haroutunian, Sensors and Actuators B 4 (1991) 545.
[18] K. Brinkman, T. Iijima, H. Takamura, Japanese Journal of Applied Physics Part2: Express Letters 46 (2007) L93.
[19] C. Michel, J. Moreau, G. Achenback, R. Gerson, W. James, Solid State Communications 7 (1969) 701.
[20] Y. Takeda, K. Kanno, T. Takada, O. Yamamoto, M. Takano, N. Nakayama, Y. Bando, Journal of Solid State Chemistry 63 (1986) 237.
[21] C. Yang, J. Seidel, S. Kim, P. Rossen, P. Yu, M. Gajek, Y. Chu, L. Martin, M. Holcomb, Q. He, P. Maksymovych, N. Balke, S. Kalinin, A. Baddorf, S. Basu, M. Scullin, R. Ramesh, Nature Materials 8 (2009) 485.
[22] S. Selbach, M. Einarsud, T. Grande, Chemistry of Materials 21 (2009) 169.
[23] Teijin Ltd., Jpn. Kokai Tokkyo Koho, 812404 (1981).
[24] S. Li, Y. Cong, L. Fang, W. Yang, L. Lin, J. Meng, Y. Ren, Materials Research Bulletin 33 (1998) 183.
[25] J. Li, Y. Duan, H. He, D. Song, Journal of Alloys and Compounds 315 (2001) 259.
[26] Z. Shao, G. Xiong, Y. Cong, W. Yang, Journal of Membrane Science 164 (2000) 167.
[27] B. Cullity, Elements of X-ray Diffraction, ISBN: 0201610914 publisher Prentice Hall 3 rd edition (2001).
[28] ρ_{xray} calculated as mass/volume: the estimated mass for ABO_3 perovskite unit cell assumed that Sr and Bi ions occupy only the A site due to ionic radius (1 A site per unit cell), Fe occupies the B site (1 B site per unit cell) and assumed perfect oxygen stoichiometry (3 oxygen's per unit cell); the estimated volume was calculated from X-ray data based on $V_{cubic} = a^3$, and $V_{rhomb} = a^3\sqrt{1-3cos^2pha + 2cos^3\alpha}$.
[29] C. Wagner, Zeitschrift fur Physikalische Chemie B 21 (1933) 25.
[30] K. Brinkman, T. Iijima, K. Nishida, T. Katoda, H. Funakubo, Ferroelectrics 357 (2007) 599.
[31] Y.-M. Chiang, E. Lavik, I. Kosacki, H. Tuller, J. Ying, Applied Physics Letters 69 (1996) 185.
[32] F. Poulsen, G. Lauvstad, R. Tunold, Solid State Ionics 72 (1994) 47.
[33] A. Markov, M. Patrakeev, O. Savinskaya, A. Nemudry, I. Leonidov, O. Leonidova, V. Kozhenvikov, Solid State Ionics 179 (2008) 99.
[34] J. Van Roosmalen, E. Cordfunke, Journal of Solid State Chemistry 93 (1991) 212.